AIAA AVIATION Forum
June 27-July 1, 2022, Chicago, IL & Virtual
AIAA AVIATION 2022 Forum

10.2514/6.2022-3926

High-Frequency Pulsed Co-axial Injectors for High-Speed Flow Mixing and Control

John T. Solomon[1], Rhys Lockyer[2], Tailor Jones[3]
Tuskegee University, Tuskegee, AL, 36088

Philip Kreth[4]
University of Tennessee Space Institute, Tullahoma, TN 37388

Efficient and controlled mixing of fuel with fast-moving air is a challenging physical problem relevant to hypersonic systems. Although mixing happens at the molecular level through diffusion, the macroscopic phenomena such as entrainment and vorticity dynamics resulting from the shear layer instabilities of the mixing fluids play a significant role in the overall efficiency of the process. With a focus on improving mixing at extreme flow conditions, this paper presents a fundamental study of a novel, high-speed, pulsed co-flow system integrated with ultra-high frequency actuators that operates at 11-20 kHz. This injection system consists of a supersonic actuation air jet at the inner core that provides large mean and fluctuating velocity profiles in the shear layers of a fluid stream injected surrounding the core through an annular nozzle, with pulsing occurring at a designated frequency. The high-frequency streamwise vortices and shockwaves tailored to the mean flow significantly enhanced supersonic flow mixing between the fluids compared to a steady co-axial configuration operating at the same input pressure. Experiments also indicate a strong connection between the frequency and unsteady amplitude of the actuation jet to the supersonic flow mixing phenomena. This paper reports the design details of the injector assembly and flow mixing characteristics captured using phase-locked microschlieren and planar laser-induced fluorescence (PLIF) techniques.

I. Introduction

The efficient mixing of two fast-moving fluid streams is a crucial engineering problem in high-speed combustion systems. Several aerospace applications use a co-axial jet configuration, a simple and effective mixing method in which fluids flowing separately through the inner core and the annular space meet at the exit plane of the nozzle assembly. For example, in applications like a gas turbine or combustion chamber of a rocket engine, these fluids could be oxidizers, such as gaseous or liquid oxygen, and fuel in its liquid or gaseous phase. Effective and controlled mixing can lead to higher combustion efficacy, longer life, reduced combustor size, stable operations, and fewer emissions/pollutants. Although the mixing ultimately happens at the molecular level, active flow control techniques can tailor the flow dynamics at micro and macro scales in favor of rapid diffusion at the molecular level [1-3].

The microscopic convective time scale (order of milliseconds) associated with hypersonic flow systems demands effective fuel injection techniques for their efficient and stable operations. There is a need for robust flow control actuators to enhance microscale mixing at high-speed and positively alter the macroscopic phenomena involved. The entrainment and vorticity dynamics resulting from the shear layer instability modification play a significant role in the overall efficiency of the mixing process. Since mixing and control face more challenges in

[1]Associate Professor, Department of Mechanical Engineering, Senior Member AIAA

[2,3] Research Assistant

[4]Assistant Professor, Department of Mechanical, Aerospace, and Biomedical Engineering, UTSI

extreme flow conditions, feasible solutions are critical to advancing next-generation air-breathing hypersonic flight systems. Passive methods proposed for improved mixing use flush mounted or intrusive injectors to generate streamwise, counter-rotating vortices for rapid nearfield mixing of the incoming air and fuel [4-12]. Beyond the classical passive co-axial configurations, a few studies explore active schemes such as powered resonance tubes (PRT) or Hartmann-Sprenger tubes as an option to excite the shear layer at high frequency [13]. Studies show that such active jet modulation is promising for improving penetration and high-speed mixing compared to unmodulated jets. However, the limited operational bandwidth and larger size restrict their implementation in practical systems.

The current paper presents the design and experimental studies on an active co-axial injector configuration, as shown in Fig. 1. This design could tailor the instabilities of an injected co-flowing fluid using a pulsed supersonic air jet blasting up to 20 kHz with a bandwidth of 10 kHz. The injector assembly shown in Fig. 1 has four major components: 1) an under-expanded source jet from a steel tube of 1.5 mm diameter enters 2) an injector assembly made of three plates with internal cavities fabricated with the desired cavity volume of 20.3 mm^3, and 3) another steel tube (1 mm ID, 1.5 mm OD) that allows pulsed jet flows out of the cavities, and 4) a separate fluid passage that opens up around the 1 mm steel tube through a circular orifice of 1.95 mm diameter forming an annular space at the exit of the assembly. This annular space forms a circular slit with a 1.5 *mm* radius and a thickness of 230 micrometers, as indicated in fig. 1. This co-axial annular orifice injects a steady fluid stream while the central steel tube exit a pulsed actuation air jet. Both the fluids meet co-axially at the exit plane of the assembly, as demonstrated in fig 1.

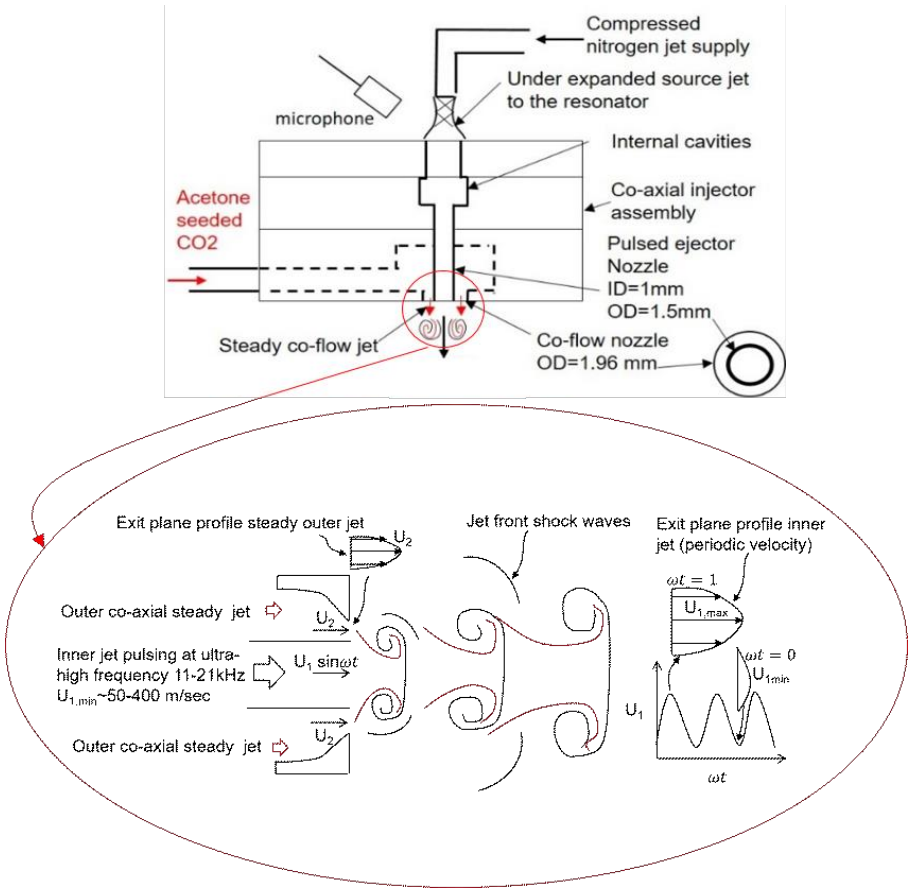

Fig. 1 Schematic of the pulsed co-axial injector assembly used in this study

Fig. 1 also shows representative flow patterns of the flowfield at the exit of the nozzle assembly when the steady co-axial jet interacts with the central actuation jet. The inner jet velocity U1 has a periodic variation from ~10-400 m/sec, and it generates a highly unsteady velocity profile at the exit, as indicated in fig. 1. The co-axial annular stream exit with a constant velocity of U2 depending on the injection pressure. Its shear layer is exposed to ambient air and the central pulsing jet on the other side. The high frequency, pulsed supersonic jets generated uses

an actuator design developed by Solomon et al. [14-19] for various high-speed flow control applications. Under suitable geometric and flow conditions, this design can generate unsteady supersonic jets over a large bandwidth of 1-60 kHz. Section 2 discusses more design details of the co-axial injector assembly and the mechanism of generating the ultra-sonic, supersonic pulsed jet.

The actuation jet exiting the nozzle assembly generates high-frequency pulsed compressible vortexes and shockwaves. The fluid injected through the outer core will get entrained into this fast-moving vortex and diffuses into it as it travels downstream. These vortexes and shockwaves excite the shear layer of annular flow on micro and macro scales, causing enhanced mixing between them. The ongoing work aims to understand the flow dynamics of this pulsed co-axial assembly using specially designed phase-locked microschlieren imaging and quantitative measurements using laser-induced fluorescence (PLIF). PLIF is a non-invasive measurement technique. It is suitable for quantifying the mixing characteristics of acetone seeded annular jets that interact with high-frequency pulsed actuation air-jet and the surrounding ambiance.

The PLIF method used in this study uses a thin laser sheet of 266 nm wavelength to fluoresce the absorbing species (acetone) in a given measurement volume. Many studies report that acetone fluorescence has a linear variation with concentration and laser power [20-21]. Acetone absorbs ultraviolet light (225 - 320 nm) but fluoresces in the blue (350 - 550 nm). This study uses CO2 as an annular stream and compressed nitrogen for generating high-frequency actuator jet pulses. Since the resulting fluorescence is proportional to the amount of the absorbing species in the measurement volume, measuring the intensity of light from the fluorescent molecules captured using an appropriate camera with a filter will quantify the mixing. The mixture fraction calculated at each location usually represents the mixing characteristics of the flow.

II. Experimental Details

A. Facility Description

a) Microschlieren system

The experiments presented in this paper were conducted in the microscale flow diagnostic laboratory at Tuskegee University with support from the US National Science Foundation. The experimental setup consists of a vibration-free optical table equipped with state-of-the-art data acquisition and flow imaging systems, as shown in figure 2. Figure 3 shows a photograph of the experiment setup with all components marked.

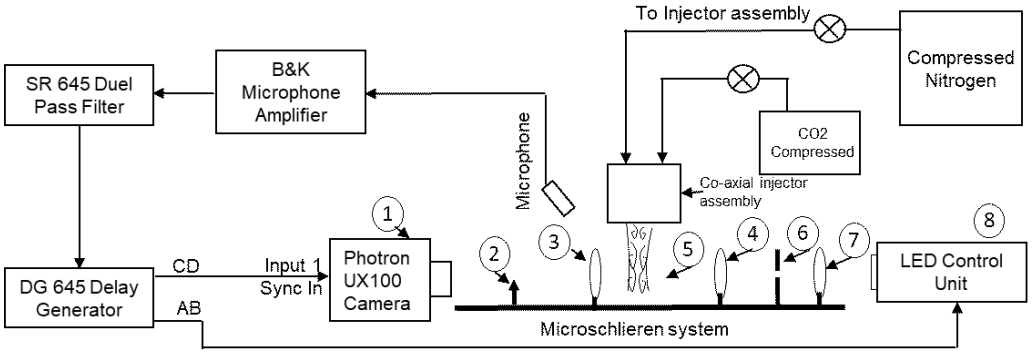

Fig. 2 Experimental setup used for microschlieren imaging used in the present study

The phase-locked microschlieren image acquisition uses a Photron mini^{TM} high-speed camera. This monochromatic camera captures up to 4000 frames per second at its full resolution of 1280x1024 pixels. A lens-based microschlieren system shown in Fig. 3 has been set up on the optical table for visualizing the microscale supersonic flowfield of the active nozzle assembly. The light source in this microschlieren system uses a custom-made LED and circuit that provides white light with a pulse width of 80*ns*. Such a light source with an extremely short pulse duration allows 'freezing' and capturing the high-speed microscale compressible flow structures generated by the active nozzle assembly.

In the microschlieren system, a light from the LED is focused onto a sharp rectangular aperture using a condensing lens. A 60 mm lens collimates, and another focuses this beam to the edge of a sharp knife and cuts the

image intensity to half. A camera lens positioned at an appropriate distance captures the image of the flowfield kept in test section 5, as indicated in Fig. 3. The pulsing frequency of the actuator is measured using a Grass microphone. Another microphone (B&K) with an amplifier generates signals for phase-locked measurements. This signal goes to an SR645 duel pass filter before generating frequency divided, pulsed square waves CD and AB using a DG 645 delay generator with an appropriate delay between the pulses. These signals trigger the camera and the LED light source for phase-locked measurements. A high-pressure compressed nitrogen tank (2000 psi) supplies air to the source jet nozzle coupled to the pulsed jet injector assembly. Compressed CO2 gas was used as the co-axial stream for microschlieren flow visualization studies. A multi-channel oscilloscope monitors all signals used for measurements for accuracy.

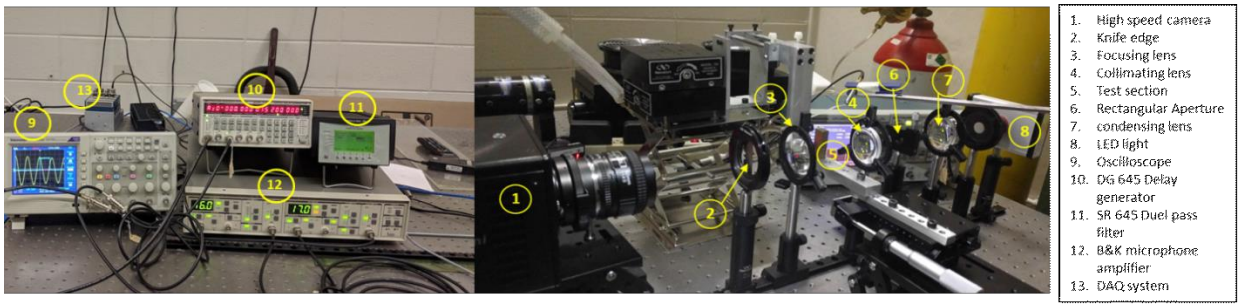

Fig. 3 Microschlieren imaging and DAQ setup used for phased locked flowfield visualization

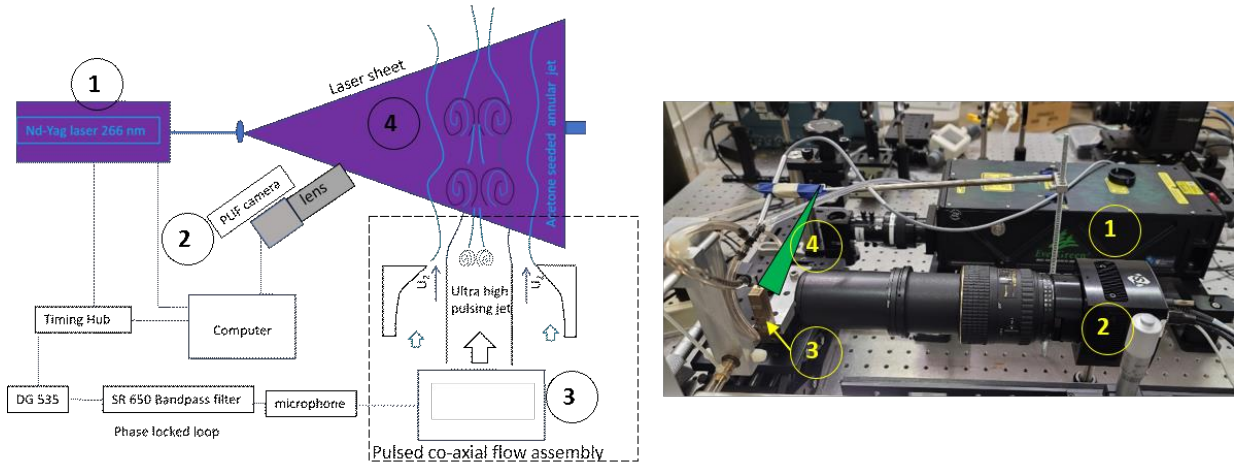

a) b)

Fig. 4 PLIF measurement system established at Tuskegee University a) various components of PLIF b) photograph of PLIF components

b) Set up for planar laser-induced fluorescence (PLIF)

The PLIF imaging uses a setup, as shown in Fig. 4, established at Tuskegee University. The critical component of this setup is a Quantel EverGreen^{TM} Nd-YAG dual pulsed laser with a choice of pulse energies up to 200 *mJ* at 532 nm and 30 *mJ* at 266 nm with a repetition rate of 15 Hz. PLIF experiments use laser pulses at 266*nm.* A Powerview^{TM} LS-LCD camera (29 MP, 6600x4400), with high quantum efficiency, low noise with 1.8 frames/s, selectable 12-bit or 14-bit output, and 100 mm f/2.8 macro camera lens, acquires the images. An eight-channel digital laser pulse synchronizer with 250 *ps* resolution controls the laser pulses and the trigger for the camera. A UV optic periscope and adjustable laser sheet optics (LSO) with 266/532 mm AR coat create a thin laser sheet at an appropriate test plane in the flowfield generated by the pulsed co-axial assembly. A six jet oil droplet generator creates saturated acetone vapor in CO2 gas, the seed fluid stream used for mixing experiments. The image acquisition and analysis use INSIGHT4G^{TM} software. Figure 4*b* shows a photograph of the PLIF imaging setup established for this study.

c) Measurement of nearfield spectra of actuator flowfield

The unsteady spectra of the flowfield of the active nozzle assembly were measured using a GRAS™ 1⁄4-inch Free-Field Microphone with a sensitivity of 4 *mV/Pa*. National Instruments™ 9234, 24-bit, 51.2 kHz data-acquisition module acquires the microphone data using LabVIEW™. Fast Fourier transformation (FFT) of time series with 2048 data points and Hanning window with 50% overlap compute acoustic spectra used in the analysis. The source jet pressure measurement has an uncertainty of 0.1 psi. The micro-gauge used for linear movements of the nozzle block, for varying the parameter *h/d*, has an uncertainty of ±0.01 mm. A TSI™ mass flow multi-meter 5300-4 measures the flow rate of acetone seeded CO2 with 2% reading accuracy for measurements up to 300L/min.

B. Design details of the co-axial injector assembly

Figure 5 shows the design details of the pulsed co-axial injector assembly fabricated with three separate brass plates. The top plate contains a 3mm long, 1.3 mm diameter cavity through which an under-expanded actuator source jet enters the nozzle block. The second plate has another internal hole that forms the boundary for the resonance phenomena. 1 mm (ID) steel tube (with 1.5 mm OD) connects the cavity in the second plate and directs the air jet to flow out from the base of the third plate. The last plate has a 1.96 mm orifice so that when combined with the second plate and the steel tube with 1.5 mm OD, an annular space is formed outside the 1mm tube (ID). The internal cavity in plate 3 connects to a steady fluid (CO2) supply line through a steel tube. The design ensures no interaction or coupling between the co-axial fluids before they reach the exit plane of the assembly.

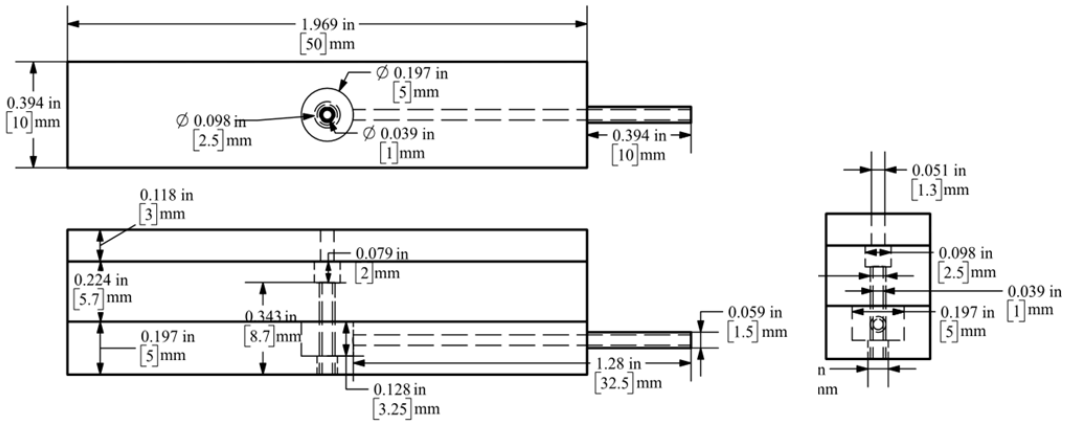

a) Front and top view *b)Side view*

Fig. 5 Design details of the co-axial injector used in this study a) Front and top view b) side cross-sectional view

This assembly has a total internal cavity volume of 20.6 mm^3. An under-expanded source jet supplied from a nozzle of 1.5 mm exit diameter (*d*) enters the assembly through a 1.3 mm orifice located on the first plate. This source jet produces pulsed flow through the 1mm diameter tube integrated into the second and third plate under suitable resonance conditions. This design allows acetone seeded fluid stream (CO2) injection through the annular space while the central tube delivers a pulsed actuation jet (N2). Figure 6 shows the top and bottom views of the nozzle assembly. Experiments use two parameters, *h/d* or nozzle pressure ratio, *NPR,* where *h* is the distance of the exit point of the source jet to the actuator cavity and *d* is the source nozzle diameter, for frequency control. The present study uses *h/d* from 1.0 to 1.6 and NPR from 5.8 to 5.5.

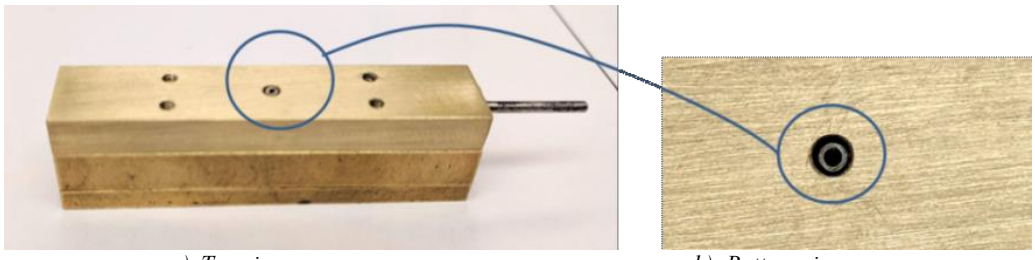

a) Top view *b) Bottom view*

Fig. 6 Photograph of the pulsed co-axial injector *a*) Top view *b*) central nozzle exit surrounded by annular space

III Results and Discussions

a) Frequency characterization of the pulsed co-axial assembly

Figure 7 shows the frequency spectra of the actuator integrated into the nozzle assembly measured using the Grass™ microphone that picks acoustic signals from the nearfield. Figure 1 indicates the microphone's location, 40mm away from the source jet, oriented at an angle of 45° from the vertical. Acoustic data shows that the pulsing frequency varies from 15 to 20 kHz by varying parameter *h/d* from 1.0 to 1.6, at a constant value of *NPR* = 5.8. A second microphone (B&K) simultaneously generates real-time signals for phase-locked imaging of the flowfield. A frequency-divided and filtered signal input to the DG645 delay generator outputs digital pulses with appropriate delay (trigger signals) for camera and LED light sources. Section IIA discussed more details of this measurement and the data processing method used for generating the acoustic spectra.

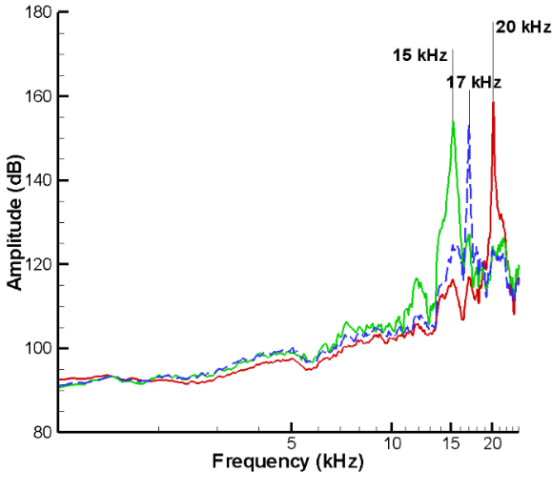

Fig. 7 Frequency spectra of the pulsed co-axial assembly

b) Frequency characterization using high-speed Schlieren images

Apart from microphone measurements, the frequency of the actuator assembly is measured using a high-speed schlieren imaging technique at the University of Tennessee Space Institute (UTSI). Fig. 8*a* shows several temporal schlieren images of the global flowfield captured with a camera operating at 200,000 frames/second. These images indicate the flow structures of the actuation jet and the oscillations of the driving source jet. Note that every time-resolved images treat each pixel as an individual measurement of the fluctuating content present within the flow. Fig. 8*b* shows the results from computing the spectra of each pixel and averaging these spectra across the entire image domain. The dominant peak located at approximately 20 kHz is the frequency at which the actuator resonates. Image shown in Fig. 9 maps this high-amplitude peak by considering each pixel independently. Here, the contour levels, which are representative of the normalized intensity of the fluctuating content, appear centered around the 20 kHz peak. These two distinct frequency measurements, one using a microphone and the other using the time-resolved Schlieren technique, confirm the ultra-sonic frequency excitation capability of the actuator integrated into the co-axial nozzle assembly.

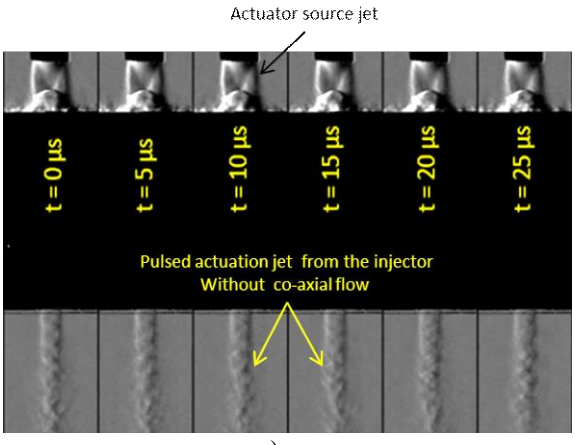

a)

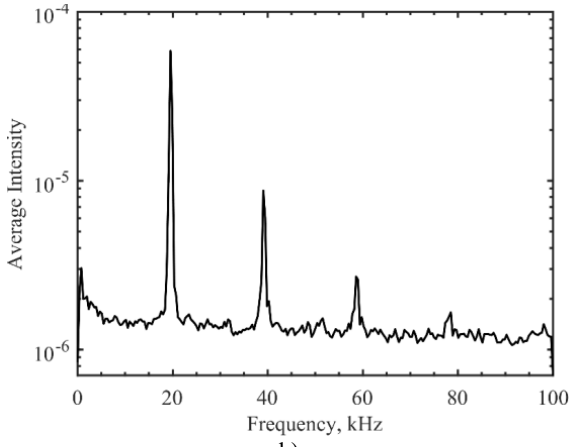

b)

Fig. 8 a) Typical sequence of instantaneous Schlieren images obtained at 200,000 fps b) Reduction of the time-resolved image sequences to spectral content averaged over the entire imaging domain.

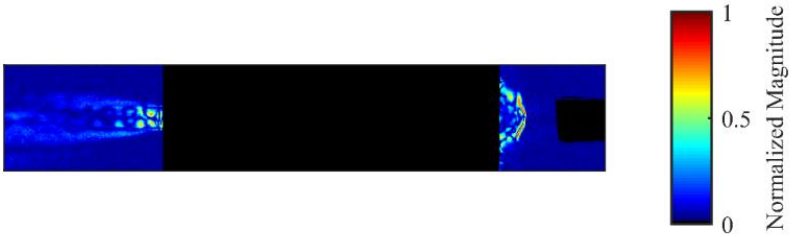

Fig. 9 Contour mapping of the relative intensity of the 20 kHz peak from Schlieren images

c) Phase-locked flowfield of the actuator and co-axial jets

Fig. 10 shows eight phase-locked, instantaneous images of the actuation jet for a cycle (360°) operating at 15.5 kHz without a co-axial CO2 stream. Each of these images is 45° phase angle apart and 8-microsecond time interval. These images capture various phases of the evolution of the pulsed supersonic actuation jet in the co-axial injector assembly. The structures indicate that the flow is supersonic in the first 5 phases, nearly sonic in the 6th phase, and low subsonic in the last two (270° and 315°). These images also indicate that the pulsed actuation generates a high-frequency compressible vortex and a blast wave in the flow field. The phase-locked images predict a vortex movement of 1.7 mm in 8 microseconds, which is the 1/8th of the period of oscillation of the phenomena (15.5 kHz) that gives an average velocity of 217 m/sec near the exit. The speed slows down to ~125 m/sec and then to 88 m/sec due to the entrainment and growth of the vortex. Our previous study using a camera with a higher frame rate and reduced resolution also reported that these vortex structures move at ~200 m/ near the exit [14]. The strength of the pulsed jet and vortex front deteriorates in the latter half of the cycle.

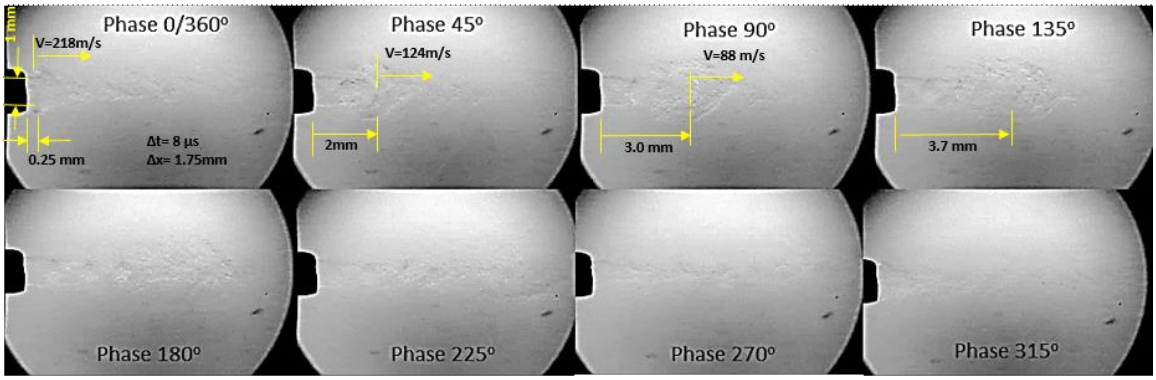

Fig. 10 Phase-locked instantaneous flowfield of central actuation jet without co-axial jet

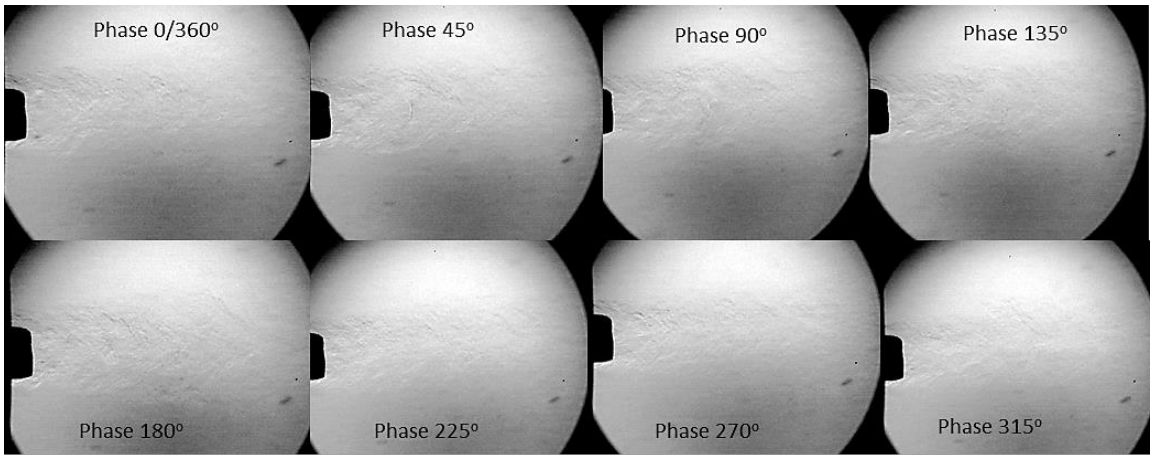

Fig.11 Phase-locked instantaneous flowfield of the co-axial jet with actuation jet

Fig. 11 shows phase-locked instantaneous images of a co-axial CO2 stream injected at a pressure of 8 psi while the actuation jet pulses at the same frequency. The characteristics of pulsed actuator flow with the injected stream are very similar to the images as shown in Fig. 10. The exit flow area ratio *A1/A2* of the present configuration is 0.72, where A1 is the area exit of actuator flow, and A2 is an area of the annular space. With a pressure ratio of fluids exiting the assembly (P_{act}/P_{stream}) that varies in the range of 1- 13 during the pulsed co-axial injection process, the momentum of the actuation jet dominates the flowfield most of the cycle.

d) Planar laser-induced fluorescence, PLIF

Fig. 12 shows an exit plane configuration of the injector assembly where an annular stream of CO2 seeded with saturated acetone vapor interacts with the unseeded compressed nitrogen jet. The present experiments use pressure and the flow rate of CO2 at 8 psi and 4.7 lit/min, respectively. For a given annular exit area of 1.24 mm^2, this flow rate gives an estimated exit velocity of U2 ~62 m/sec for the seeded CO2 jet. The exit velocity U1 of pulsed jet varies 10-400m/sec during the cycle giving rise to a velocity ratio U1/U2=0.1-6.4.

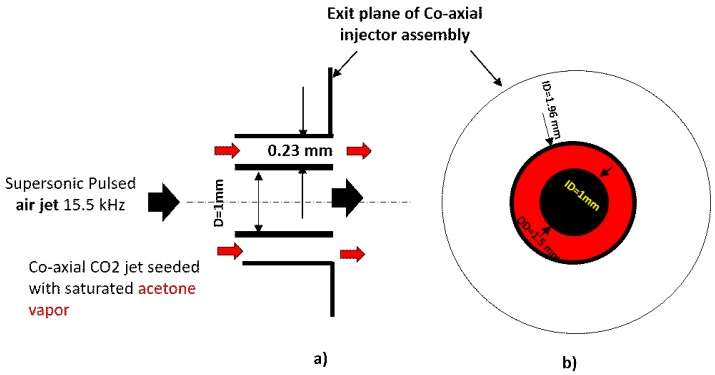

Fig. 12 PLIF configuration for seeded annular jet and unseeded actuation jet

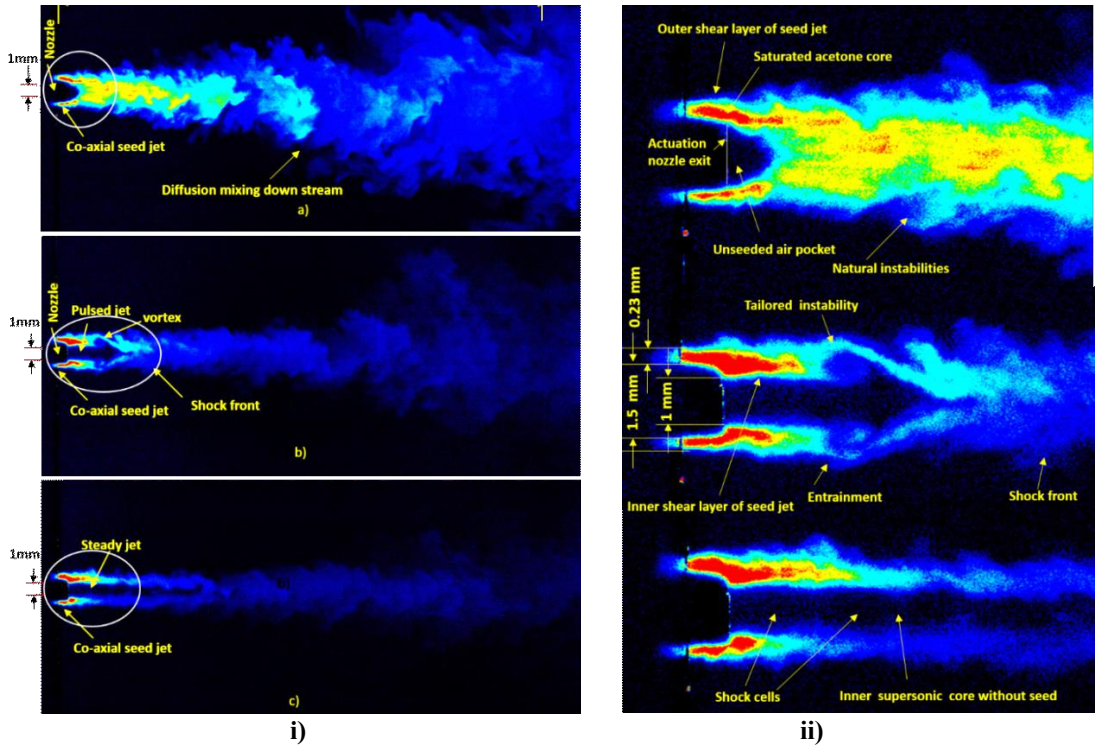

Fig.13 Instantaneous images of i) a) seed jet alone b) seeded jet + pulsed actuation jet c) seed jet+steady actuation jet ii) enlarged views at the exit

Ideally, the saturated vapor exiting the nozzle fluoresces with maximum intensity (red color) and unseeded actuation jet with zero intensity (black color). Assuming a linear variation between these two extreme values, the intensity of light fluoresce measured at a given location represents the local mixing of acetone with the surrounding unseeded streams. In the present study, we chose three configurations for the preliminary experiments: 1) A seed jet alone, 2) a seeded jet with an actuation jet pulsing at 15.5 kHz, and 3) a seeded jet with an actuation jet in a steady mode (without pulsing). Figure 13 *i) a-c* shows representative instantaneous PLIF images from these three test cases. Fig 13 *ii)* indicates a magnified flowfield near the exit with more flow features marked. The high magnification optics and a high-resolution camera (27 MP) capture fine details of these high-speed microscale flows and their mixing characteristics, as indicated in the PLIF images. For all cases, the shear layer boundaries of the seed jet and the natural instabilities present are visible and marked appropriately. For seed jet at 4.7 psi and 5 lit/min, images show the formation of a saturated core up to 10 diameters, and the jet stream seems mixed well with the ambient air further downstream by the natural diffusion mechanism. Figure 13*i) b* shows a representative phase of the flowfield when the actuator operates at 15.5 kHz. The pulsing action creates a high-frequency compressible vortex in the same frequency range. This tailored vorticity created at the inner core of the seeded jet leads to the entrainment of the seed jet to the actuator flow. The interfacial area of the vortex increases downstream, resulting in increased entrainment, diffusion, and mixing of the seeded CO2 jet with the actuation jet (N2) and the ambient air.

The moving shock front created by the pulsed vortex, as indicated in Fig 13*ii,* also improves the mixing of the seeded jet with the actuation jet and the ambient air. The inner shear layer of the seed jet experiences highly unsteady vortex movement and growth downstream. In the third case, the actuation jet operates in steady mode. This case is a classical co-axial flow configuration, as indicated in fig. 13 *i)c*. Proper control of parameter *h/d* adds or eliminates the pulsing action of the actuation jet at the same source jet pressure. In this case, the jet core without seed particles appears to be extended up to 10*d* (*d*=1mm, the exit diameter of the actuation nozzle) and then weakens. These images indicate that the compressible shear layer of the steady under-expanded jet offers more resistance to the diffusion of co-axial seed particles into the jet core. The diffusion is favorable when the jet core slows down further downstream. Figure 14 shows the microphone spectra of three cases discussed in fig. 13. The pulsed co-axial flow shows a distinct frequency at 15.5 kHz, while the steady co-axial injection shows no specific tones in the spectra other than broadband noise. In steady actuation, energy is in broadband, and it is focused at 15.5 kHz for pulsed actuation. The spectra of the seed jet show low amplitude broadband noise indicating natural instabilities exist in the flow.

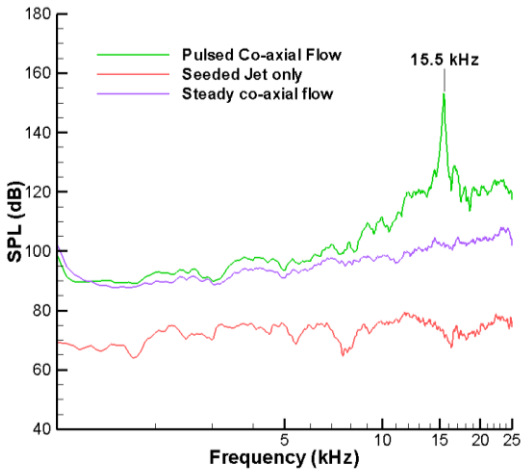

Fig.14 Spectra measured for three cases i) seed jet only a) pulsed-coaxial flow c) steady co-axial flow

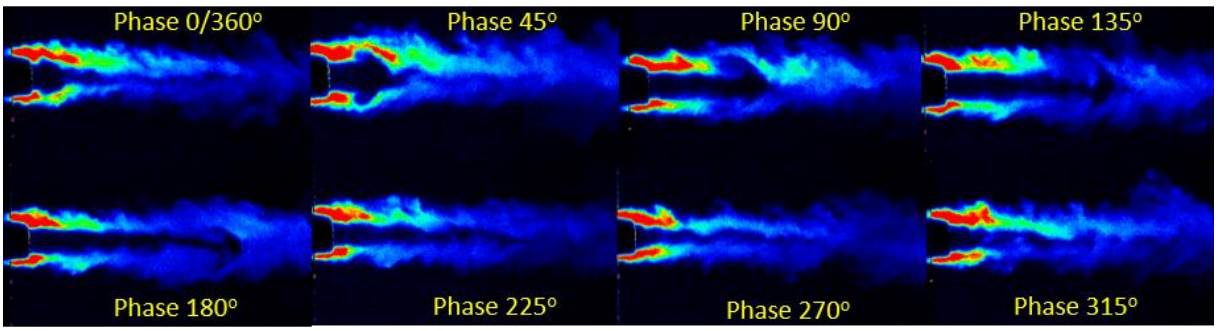

Fig.15 Eight instantaneous phases of acetone seeded CO2 jet with actuation jet pulsing at 15.5 kHz

Figure 15 shows PLIF images of co-axial flow at various phases, separated by 45°. The flow features are visibly similar to the phase-locked microschlieren images discussed in Fig. 10. These phase images provide helpful insight into the evolution and decay of the central pulsing jet and the overall dynamics of the diffusion process of the seeded annular stream. To directly compare steady and pulsed co-axial injections, Fig. 16 shows eight random images of steady injection, arranged similar to the phase images displaced in Fig. 15. Qualitatively, it is evident from Fig. 15 and 16 that the flow mixing characteristics are very distinct for steady and pulsed co-axial flow. We have noticed earlier that a steady supersonic core tends to be less effective in mixing a co-axial stream, and mixing mainly occurs downstream when the core strength deteriorates. Since diffusive mixing is directly related to the relative velocity between the fluid shear layers, the pulsed injection, which provides an opportunity for significant velocity fluctuation in the inner core of the co-axial stream, will be more effective than the steady co-axial injection. Fig. 15 and 16 confirm that pulsed co-axial injection is more effective than a regular co-axial injection for mixing under similar flow conditions.

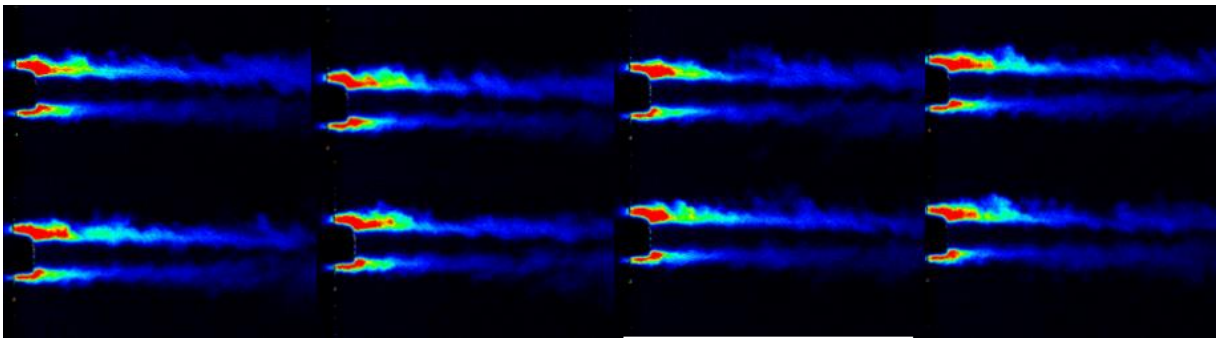

Fig.16 Eight random instantaneous images of seeded jet with steady jet actuation jet at the core

The zoomed view of the flow at the exit, as shown earlier in fig. 13, reveals the existence of a very small (±3 micrometer) asymmetry for the annular exit. The designed thickness of the annular exit is 0.23 mm, and the images show this value on the top side and 0.20 mm on the bottom side. But this asymmetry distorts co-axial flow downstream. To eliminate this asymmetry and to better understand the flow dynamics, three-phase images (45°, 180°, and 315°) were corrected for symmetry, as shown in figure 17.

Figure 17 also displays a microschlieren image of the actuation jet at the same phase angle. These images show three key characteristics: an evolving vortex, a moving shock wave, and a wavefront, which significantly impact the mixing process involved with the pulsed co-axial injection. In general, we can identify four different mixing mechanisms from these images: 1) vortex-induced mixing, 2) shock-induced mixing and 3) mixing due to growth and entrainment of vortex downstream, and 4) natural diffusion from the outer shear layer of the seeded stream. In the first mechanism, the compressible vortex formed near the nozzle exit entrains the surrounding seeded stream saturated at the nozzle exit and moving forward with a velocity of 200+m/sec. The actuation jet velocity is sonic at the nozzle exit, and it evolves as an under-expanded jet core downstream surrounded by the co-axial seeded stream. The diffusion of the seeded stream to the compressible shear layer of the jet core is minimum near the nozzle exit.

In the second shockwave induced mixing mechanism, the pulsing action produces a shock wave, as indicated in Fig. 17*a*, that moves faster than the jet front, causing breaks down of the seeded co-axial fluid shear layer ahead of it. This action creates fragmented structures with a high concentration of seed particles surrounded by the unseeded actuation jet. The moving shock drags some of these fragmented structures and its forward motion, creating a plume of disintegrated seed jet surrounded by a co-axial stream, as evident from Fig. 17*b*, causing better mixing opportunity with the ambient air. The third mixing mechanism owes to the growth and entrainment of the vortexes in the streamwise direction. In the present image data, the PLIF camera setup provides a field of view up to 30 mm in the streamwise direction and 20 mm in the spanwise direction. The images in Fig. 17*a&b* are temporally connected. For a phase angle difference of 135° (from 45° to 180°), the vortex and the wavefront move a period of 24 microseconds. Since the cycle period is 64 microseconds as measured by the spectra (15.5 kHz), the second vortex eye we see in Fig. 17*a* must be 40 microseconds separated from the wavefront seen for phase angle 180°. This vortex 2 captured in the image is the one that precedes vortex 1. The vortex 1 and vortex 2 locations are separated by a distance of 10 mm, as indicated in a scale shown in Fig. 17*a*. We can estimate an average velocity of 156 m/sec for its movement for a cycle from the nozzle exit. This estimate is close to the average velocity observations from

phased microschlieren images shown in Fig. 10.

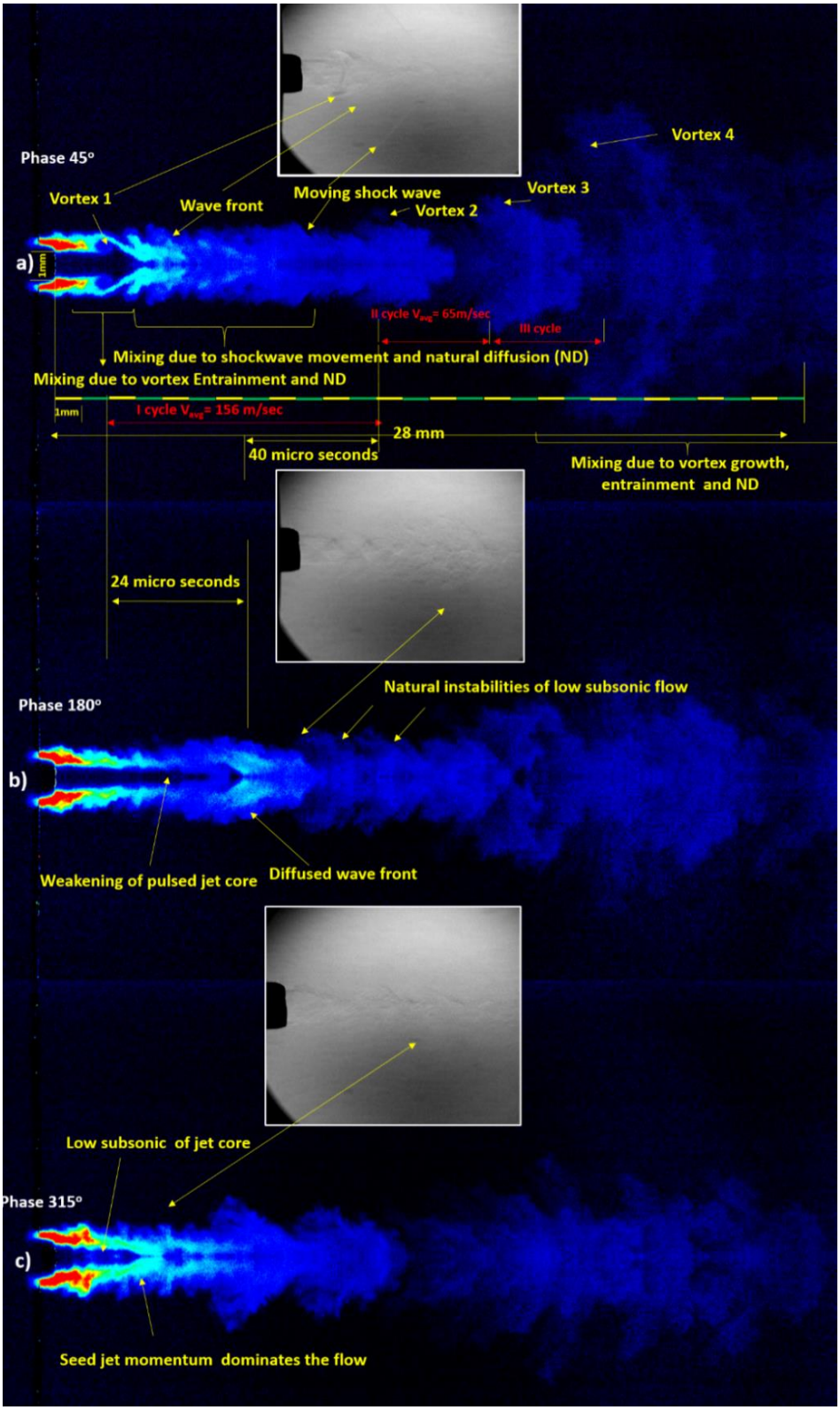

Fig.17 Symmetry correction for the flow dynamics analysis of three phases of the co-axial pulsed flowfield

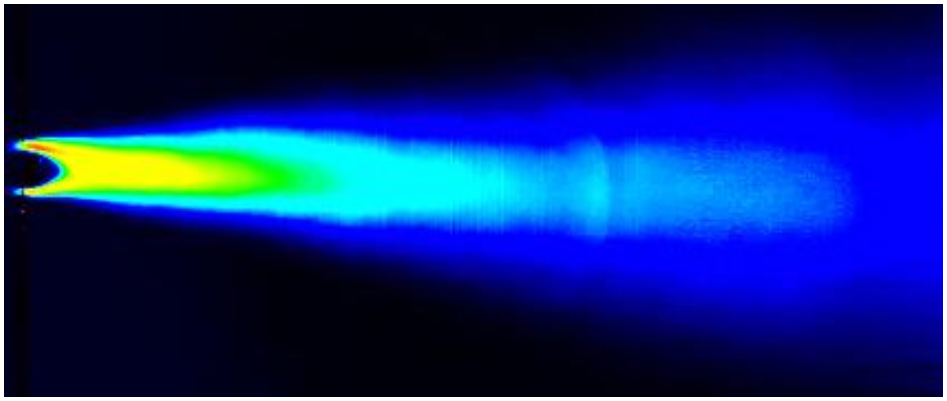

a) Seed Jet-The average intensity of pixels in the entire image – 44.3

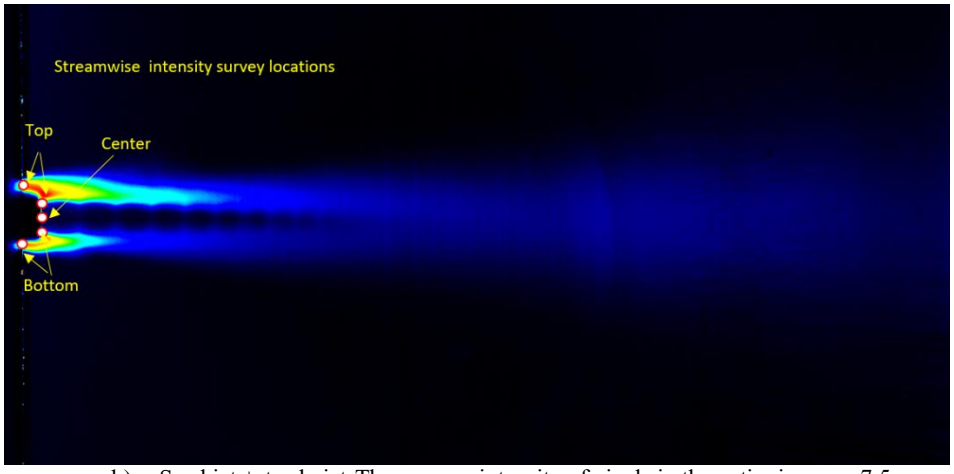

b) Seed jet +steady jet-The average intensity of pixels in the entire image – 7.5

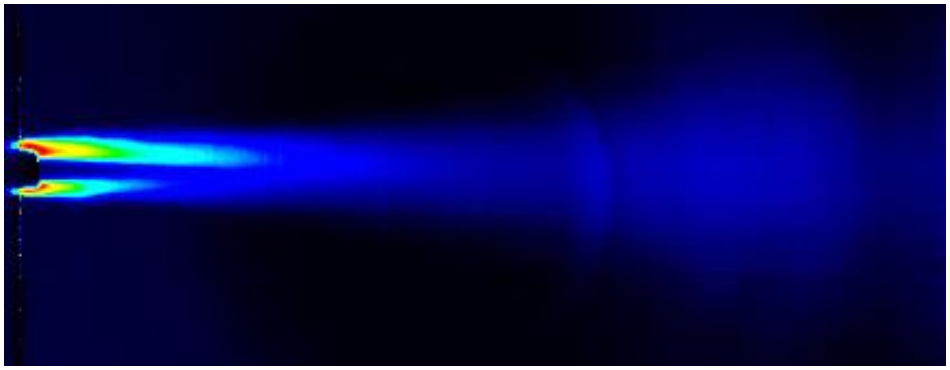

c) Seed jet + pulsed jet- The average intensity of pixels,=15.9 of the entire image, ~114% more than case b)

Fig.18 Average of 250 instantaneous PLIF images a) Seed jet alone b) Seed jet and steady actuation c) Seed jet and pulsed actuation at 15.5 kHz.

Figure 17*a* marks two more vortex eyes in the image as vortex 3 and vortex 4, which must be preceded by vortex 2 in order. The velocity estimate shows that growth and entrainment slow down to ~65 and 60 m/sec, respectively, for these two vortexes.

Finally, the fourth mechanism of mixing is the natural diffusion to the ambiance from the outer and inner shear layer of the moving vortexes and the co-axial streams. Apart from the tailored vortices numbered 1-4, the natural instability-driven vortex patterns are visible when the actuation stream slows down to subsonic speeds. Fig. 17*b* shows a weakening of the actuation core and formation of such natural vortices in the flow along with the diffused

wavefront vortex 1. In the final phases, the actuation jet momentum drops considerably so that the seeded jet momentum dominates the flow and structures. Fig. 17*c* shows that at the actuation jet's light subsonic speed, the seed jet core converges to the center, and the mixing occurs mainly due to the natural diffusion process.

Figure 18 shows averaged images for each case calculated using 250 instantaneous PLIF images. Since each instantaneous image contains information on 4-5 cycles, as discussed in Fig. 17, the average image represents information on ~1000 cycles for the pulsed injection case. These averaged images provide a comprehensive view of all three cases' mixing characteristics and provide reasonably accurate quantitative estimates of the effectiveness of mixing effectiveness between the cases. The intensity of each pixel in the averaged PLIF image is proportional to the average acetone concentration around that elemental volume for the image sequences selected. An average of all pixel intensity provides a simple estimate of acetone concentration in a given field of view for a particular case. For the first case, seed jet alone, this number is 44.3. For the second case, when an unseeded steady actuation jet flows through the core, the acetone content we measure as average intensity in the same field of view changes due to fast relative motion. The average intensity of pixels measured for this case is 7.5. The same calculation for pulsed injections shows this average intensity value as 15.9. This calculation estimate that the mixing effectiveness of pulsed co-axial injection is 114% more than the steady co-axial injection, as indicated in Fig. 19 for the same injection pressure.

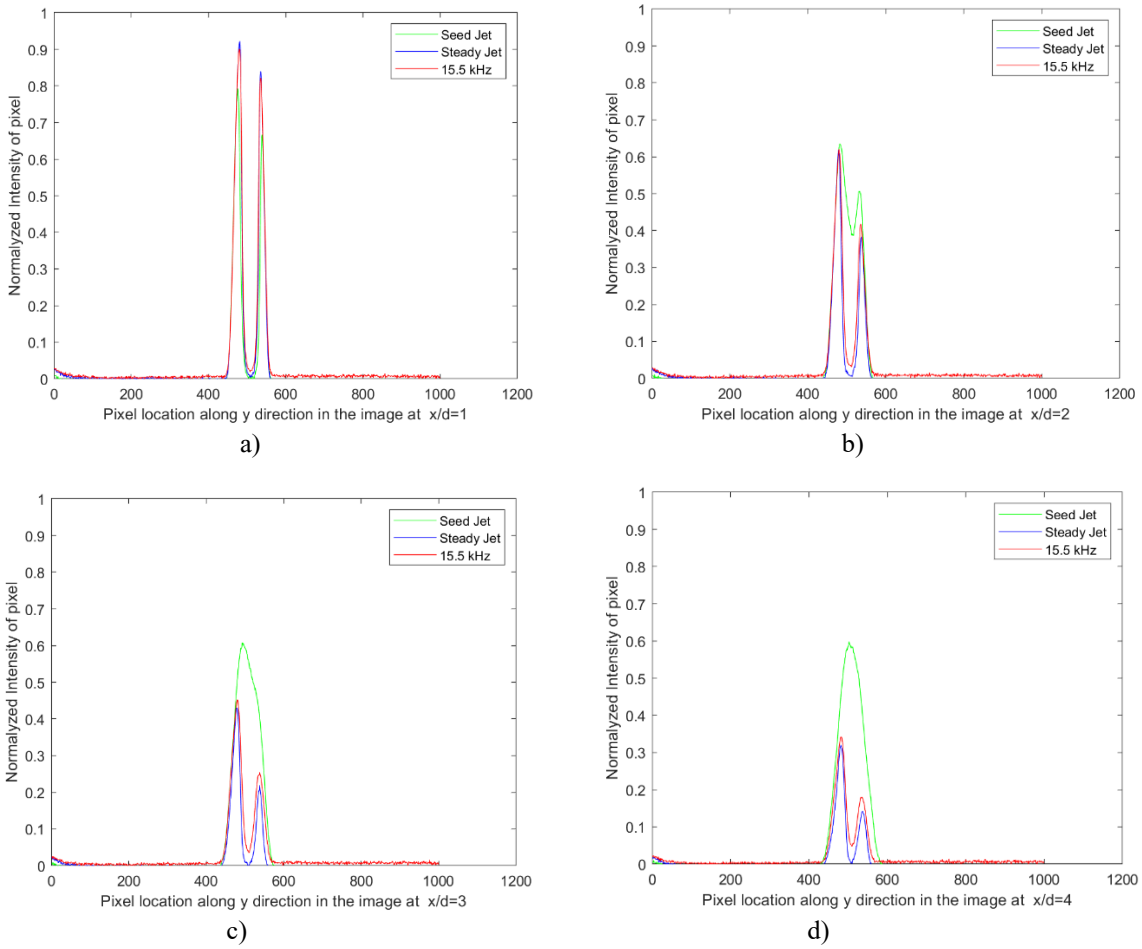

Fig. 19*a-h* shows the average intensity profiles of pixels at various streamwise locations of images shown in Fig. 18. The acetone seed jet profiles (green curve) show two maxima up to x/d=2 and then diffuses into a single jet structure. Seed density remains high in the core region, and it drops in the streamwise direction as expected. The jet width increases gradually as the jet diffuses in the downstream direction. The unseeded steady and pulsed co-axial flow (blue and red curves) profiles show two distinct peaks in all streamwise locations. A slight geometric

asymmetry at the exit nozzles creates more seeded acetone jet flow at the top side than at the bottom. Since pixel intensity directly correlates to the seed density, this results in an asymmetric intensity profile with higher intensity on the top location of the assembly indicated in Fig. 18.

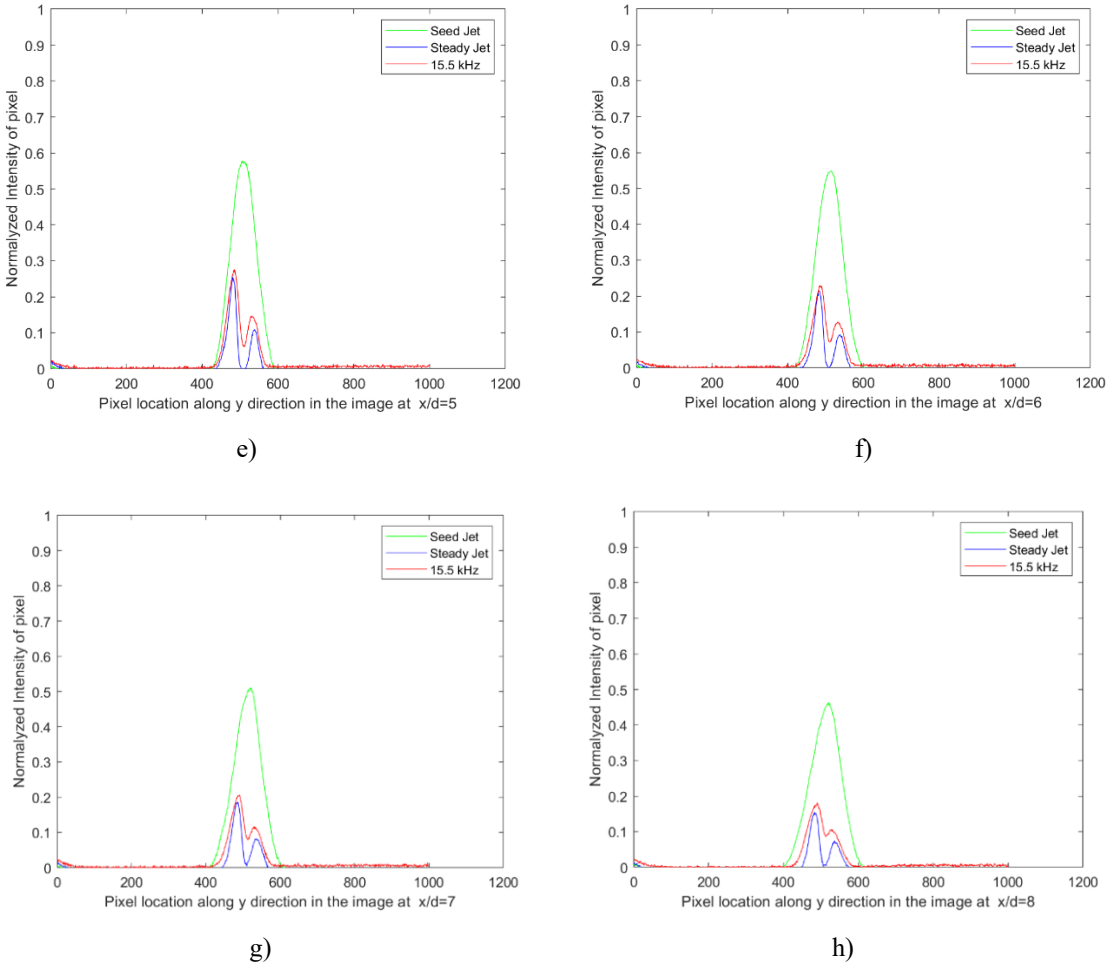

Fig.19 Normallyzed intensity profiles of averaged images shown in Fig. 18 at various x/d locations

The intensity profiles in all x/d locations indicate that the pulsed co-axial flow creates a significantly improved distribution of seeded acetone in the field of view than the steady jet operates at the same pressure. Profiles *e-h* indicate the mixing of seeded jet and the unseeded atuation jet increases as it flows downstream. As discussed earlier in Fig. 17, this enhanced mixing is attributed to the entrainment and growth of high-frequency vortex generated by the pulsed jets and through the shock wave diffusion through the interface of the seeded and unseeded flow downstream. Comparison of the jet width of steady and pulsed co-axial also gives indications of better mixing between the seeded jet and unseeded supersonic actuation jet when pulsing at 15.5 kHz. The profiles examined at various locations of x/d also reflect the mixing effectiveness of pulsed actuation estimated based on the average image intensity.

To better understand the mixing characteristics, we choose 5 locations on the exit of the injector assembly, as indicated in Fig.18*b*, the top, bottom, center, and top and bottom shear locations to plot the intensity profile along the streamwise direction. Fig. 20 represents the normalized intensity of the averaged image of the seed jet at these 5 locations. These profiles show intensity varies continuously in the axial direction. A careful look at the profiles of the seed jet indicates the intensity at the top location is high compared to the bottom side due to the asymmetry at the exit. A slight downward inclination of the seeded jet core, as evident from Fig. 18*a*, results in higher intensity values at the bottom location on the downstream side, as observed in Fig. 20*a &b*. Fig 21 and Fig. 22 show intensity

profiles of pulsed co-axial jets and steady co-axial jets at various exit locations. These profiles show the same level of intensity level near the nozzle exit.

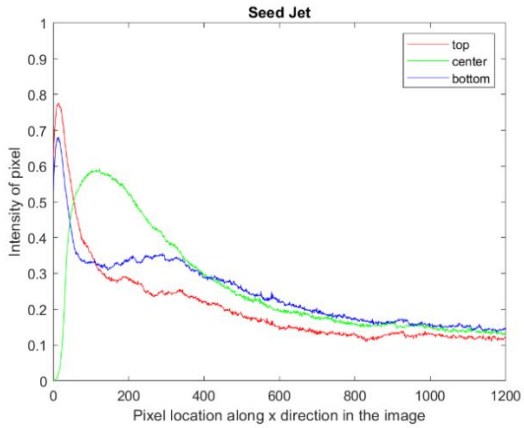

a) Top, bottom, and center locations

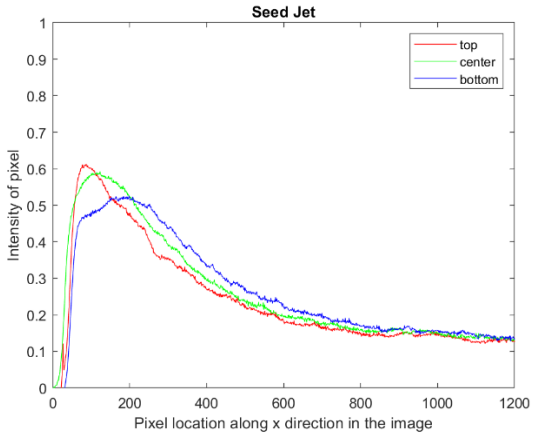

b) Shear layer location at top and bottom

Fig.20 Normallyzed intensity profiles of averaged images of Seed jet in streamwise direction at various locations

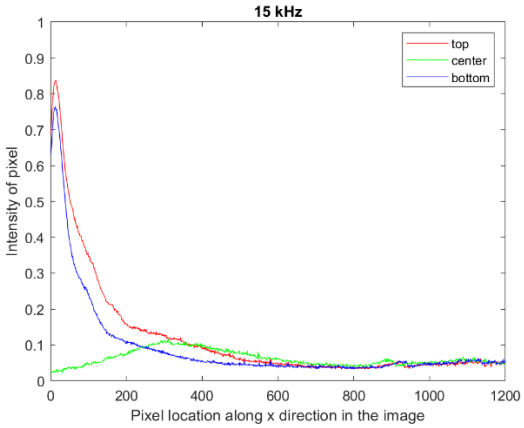

a) Top, bottom, and center locations

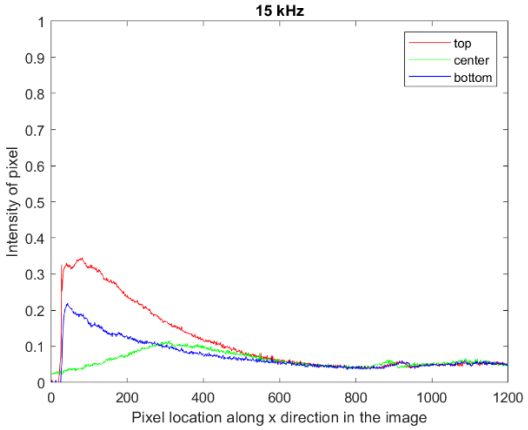

b) Shear layer locations at top and bottom

Fig.21 Normallyzed intensity profiles of averaged images of Pulsed jet in streamwise direction at various locations

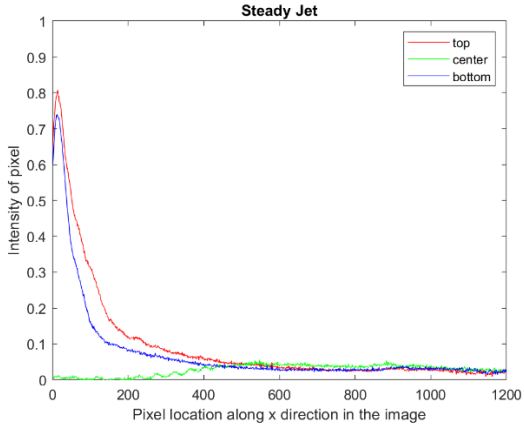

a) Top, bottom, and center locations

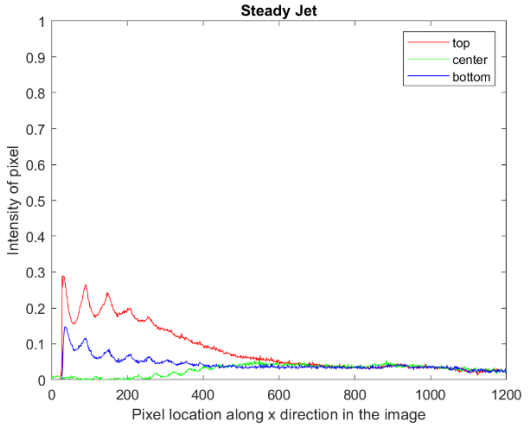

b) Shear layer locations at top and bottom

Fig.22 Normallyzed intensity profiles of averaged images of Steady jet in streamwise direction at various locations

Fig. 21*a* and 22*a* (green curve) indicate the centerline intensity in the axial direction for the pulsed and steady co-axial flow configurations. The mixing is minimum near the nozzle exit for steady co-axial flow. As evident from Fig. 21*b*, the pulsed flow provides significantly enhanced mixing near the nozzle exit for the same pressure input to the actuation source jet. Far downstream, the centerline intensity levels become similar in both configurations. A comparison of acetone intensity in the shear layer profile shown in Fig. 21 *b* and Fig. 22 *b* indicates that the pulsed co-axial actuation provides enhanced mixing characteristics in the shear layer than steady co-axial injection. The saw tooth patterns of intensity seen inf Fig. 22*b* are due to the steady jet's under-expanded jet structure at 65 psi pressure. The compressible shear layer of the jet at this high pressure offers more resistance to the diffusion across the shear layer at supersonic speed. Profiles in Fig. 22a also indicate that the higher injection pressure does not favor mixing in the vicinity of the injector.

PLIF data shows that pulsed jets operating at 15 kHz improve ~114% more mixing than a steady under-expanded jet operating in the same pressure input pressure. The experiments were conducted with an actuator operating at 11-20 kHz to understand this phenomenon further. Fig. 23 shows spectra measured for pulsed steady co-axial flow and the seed jet configuration. Another actuation case explored is actuator resonance in a broadband regime where the fluid oscillation and periodic phenomena appear in the actuator assembly. This broadband spectrum is shown in Fig. 23*b* with a black curve. The effect of this actuation on the average PLIF pixel intensity of 250 images is summarized in Fig. 24. The average pixel intensity of various configurations is 44.3, 7.4, 9.8, 11.2, 15.9, 13.1, and 11.9, respectively, for seed jet, steady jet, broadband, 11 kHz, 15 kHz, 18 kHz, and 20 kHz. The corresponding percentage change from steady jet mixing value (7.4) is 33%,50%,114%, 76%, and 60%. The highest amplitude actuation with 15.5 kHz provides the maximum value for the average intensity.

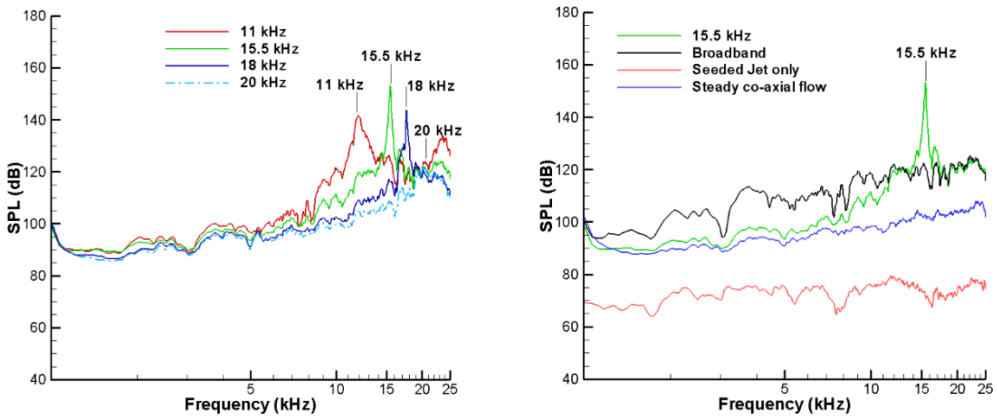

Fig. 23 Spectrum of co-axial jets used for this study a) frequency sweep of pulsed jet b) spectra of steady, broadband, and seed jet

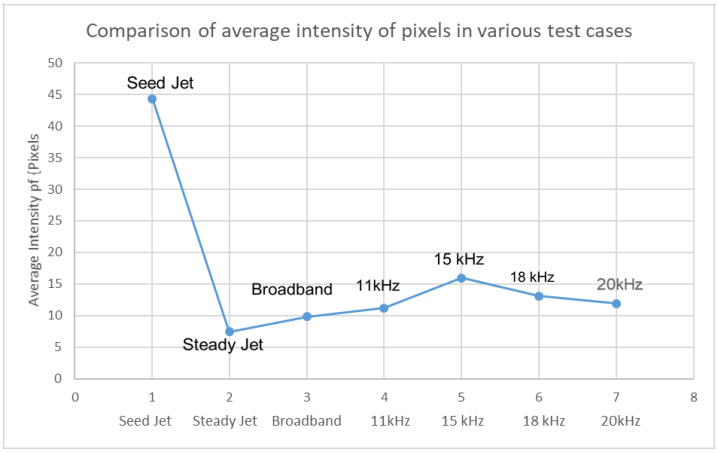

Fig. 24 Summary of the average intensity of acetone seeded stream calculated from averaged images for various test cases

IV Summary and future work

This paper reports an experimental study on an active, pulsed co-axial jet injection assembly integrated with ultra-high frequency pulsed microactuators. The assembly steadily injects a fluid through an annular space around a 1 mm nozzle through which supersonic actuation air-jet flows out at a frequency range of 11-20 kHz. The pulsed air jet develops a high-frequency compressible air vortex in the injected flowfield and entrainment of the jet injected through the annular space, causing significantly improved mixing between the two fast-moving fluids. The pulsed co-axial flowfield is analyzed using phase-locked microschlieren imaging and the planar laser-induced fluorescence (PLIF) technique. PLIF uses saturated acetone introduced to the annular jet for quantitative mixing measurements. The experimental data shows that pulsed injection enhances mixing due to vortex entrainment, shock blasting through the fluid stream, vortex growth, and natural diffusion through the outer shear layers of the flow compared to a configuration with steady actuation. The estimate shows that the compressible pulsed vortex generated by the actuation jet has an initial 216 m/sec and an average velocity of 156 *m/sec* in its first cycle close to the exit. The vortex velocity drops 65 *m/sec* after 64 microseconds. PLIF image analysis estimates that pulsed injection significantly improved mixing by 50-115% compared to steady co-axial injection under the same injection pressure conditions. The data indicate that the actuation jet's unsteady amplitude and frequency strongly influence the high-speed mixing phenomena. PIV experiments and parametric variations to these configurations are ongoing and will be reported in the future.

Acknowledgments

National Science Foundation supports this work through the grant 1900177.

References

1. B. Ritchie, D. Mujumdar, and J. Seitzman, "Mixing in co-axial jets using synthetic jet actuators," AIAA-2000-04-04.

2. Davis, S. A. & Glezer, A., "Mixing Control of Fuel Jets Using Synthetic Jet Technology: Velocity Field Measurements," AIAA Paper 99-0447.

3. Broadwell, J. E. and Mungal, M. G., "Large Scale Structures and Molecular Mixing," Physics Fluids, 1193-1206, 1991.

4. Kraus, D. K., and Cutler, A. D., "Mixing of Swirling Jets in a Supersonic Duct Flow," Journal of Propulsion and Power, Vol. 12, No. 1, 1995, pp. 170–177. doi:10.2514/3.24007

5. Cutler, A. D., and Doerner, S. E., "Effects of Swirl and Skew upon Supersonic Wall Jet in Crossflow," Journal of Propulsion and Power, Vol. 17, No. 6, 2001, pp. 1327–1332. doi:10.2514/2.5882

6. Drozda, T. G., Baurle, R. A., and Drummond, J. P., "Impact of Flight Enthalpy, Fuel Stimulant, and Chemical Reactions on the Mixing Characteristics of Several Injectors at Hypervelocity Flow Conditions," NASA Langley Research Center, May 2016, https://ntrs.nasa.gov/ archive/nasa/casi.ntrs.nasa.gov/20160009131.pdf [retrieved May 2017].

7. Gruber, M. R., Nejad, A. S., Chen, T. H., and Dutton, J. C., "Transverse Injection from Circular and Elliptic Nozzles into a Supersonic Crossflow," Journal of Propulsion and Power, Vol. 16, No. 3, 2000, pp. 449–457. doi:10.2514/2.5609

8. VanLerberghe, W. M., Santiago, J. G., Dutton, J. C., and Lucht, R. P., "Mixing of a Sonic Transverse Jet Injected into a Supersonic Flow," AIAA Journal, Vol. 38, No. 3, 2000, pp. 470–479. doi:10.2514/2.984

9. Shigeru, A., ArifNur, H., Shingo, M., Kei, I., and Yasuhiro, T., "Fundamental Study of Supersonic Combustion in Pure Air Flow with Use of Shock Tunnel," Acta Astronautica, Vol. 57, Nos. 2–8, 2005, pp. 384–389. doi:10.1016/j.actaastro.2005.03.055

10. Menon, S., "Shock Wave Induced Mixing Enhancement in Scramjet Combustors," AIAA Paper 1989-0104, 1989. doi:10.2514/6.1989-104 [

11. Ben-Yakar, B., Mungal, M. G., and Hanson, R. K., "Time Evolution and Mixing Characteristics of Hydrogen and Ethylene Supersonic Crossflow," Physics of Fluids, Vol. 18, No. 2, 2006, Paper 026101. doi:10.1063/1.2139684

12. Hsu, K., Carter, C. D., Gruber, M. R., and Tam, C., "Mixing Study of Strut Injectors in Supersonic Flows," AIAA Joint Propulsion Conference, AIAA Paper 2009-5226, 2009. doi:10.2514/6.2009-5226

13. Hongbin, G., Zhi, L., Fei, L., Lihong, C., Shenglong, G., and Xinyu, C., "Characteristics of Supersonic Combustion with Hartmann-Sprenger Tube Aided Fuel Injection," AIAA Conference, AIAA Paper 2011-2326, 2011. doi:10.2514/6.2011-2326

14. Solomon, J. T., Cairnes, K., Nayak, C., Jones, M. and Alexander, D. Design and Characterization of Nozzle Injection Assemblies Integrated High-frequency Microactuators. AIAA Journal Vol. 56, No. 9, pp. 3436-3448, 2018.

15. Ali MY, Arora N, Topolski M, Alvi FS, and Solomon JT. Properties of Resonance Enhanced Microjets in Supersonic Crossflow" AIAA Journal, AIAA Journal, Vol. 55, No. 3, pp. 1075-1081. https://doi.org/10.2514/1.J055082, 2017.

16. Uzun, A., Solomon, J.T., Foster, C.H., Oates, W.S., Hussaini, M.Y., Alvi, F.S. Flow physics of a pulsed microjet actuator for high-speed flow control. AIAA Journal Volume 51, No. 12, pp 2894-2918, 2013.

17. Solomon, J. T., Foster, C., Alvi F.S. Design, and characterization of High-Bandwidth, Resonance Enhanced, Pulsed Microactuators: A parametric study. AIAA Journal, Volume 51, No. 2, pp 386-396. , 2013.

18. Solomon, J. T., Kumar, R., and Alvi, F.S. High-Bandwidth Pulsed Microactuators for High-Speed Flow Control," AIAA Journal, Vol. 48, No. 10, pp. 2386-2396, doi.org/10.2514/1.J050405, 2010.

19. Solomon, J, T. High-bandwidth Unsteady Actuators for Active Control of High-Speed Flows," Ph.D. Dissertation, Florida State University. http://purl.flvc.org/fsu/fd/FSU_migr_etd-1642, 2010.

20. Lozano, A., Smith, S. H., Mungal, M. G. and Hanson, R. K., "Concentration Measurements in a Transverse Jet by Planar Laser-Induced Fluorescence of Acetone" AIAA Journal 32, 218-221, (1994).

21. Lozano, A., Yip, B., and Hanson, R. K., "Acetone: a by planar laser-induced fluorescence," Experiments in Fluids 13, 369-376, (1992)